








The Impact of a Southern Ocean Cyclonic Eddy on Mesopelagic Micronekton

Alice Della Penna^{1,2} , Joan Lloret³ , Sebastien Moreau⁴ , Ramkrushnbhai Patel^{5,6} , Rudy Kloster⁷, Peter Gaube⁸ , Peter Strutton^{5,6} , and Philip W. Boyd⁵ 

¹Institute of Marine Science, University of Auckland, Auckland, New Zealand, ²School of Biological Sciences, University of Auckland, Auckland, New Zealand, ³Barcelona Supercomputing Center, Barcelona, Spain, ⁴Norwegian Polar Institute, Fram Center, Tromsø, Norway, ⁵Institute for Marine and Antarctic Studies (IMAS), University of Tasmania (UTas), Hobart, TAS, Australia, ⁶Australian Research Council Centre of Excellence for Climate Extremes, University of Tasmania, Hobart, TAS, Australia, ⁷CSIRO Oceans and Atmosphere, Hobart, TAS, Australia, ⁸Applied Physics Laboratory, University of Washington, Seattle, WA, USA

Key Points:

- We observed the distribution of acoustic backscatter in the mesopelagic zone across a Southern Ocean cyclonic eddy
- The integrated and vertical distribution of the acoustic backscatter inside the eddy were similar to its origin waters
- The eddy presented a unique habitat compared to its surrounding waters, affecting the accessibility of mesopelagic prey to diving predators

Supporting Information:

Supporting Information may be found in the online version of this article.

Correspondence to:

A. Della Penna,
alice.dellapenna@gmail.com

Citation:

Della Penna, A., Lloret, J., Moreau, S., Patel, R., Kloster, R., Gaube, P., et al. (2022). The impact of a Southern Ocean cyclonic eddy on mesopelagic micronekton. *Journal of Geophysical Research: Oceans*, 127, e2022JC018893. <https://doi.org/10.1029/2022JC018893>

Received 25 MAY 2022

Accepted 28 OCT 2022

Abstract Mesoscale eddies shape the foraging ecology of predators such as marine mammals and seabirds. A growing number of animal tracking studies show that predators alter their swimming, diving, and foraging behavior within mesoscale eddies. However, little is known about how Southern Ocean eddies influence the distribution of mesopelagic micronekton (fish, squid, and crustaceans), which are major prey items of megafauna. Studies in other oceanic regions have found that eddies can influence the abundance and community composition of micronekton. Here, we analyze acoustic observations from a 14-day survey of a cyclonic mesoscale eddy, its surrounding waters, and the Polar Frontal Zone (PFZ) waters where the eddy formed. We report and interpret spatial patterns of acoustic backscatter at 18 and 75 kHz, proxies indicating combined changes in species, size, and abundance of micronekton. We find that the vertical distribution of acoustic backscatter matched the underwater light conditions characteristic of the eddy core, periphery, and surrounding waters, at scales smaller than 10 km. The median water-column integrated acoustic backscatter values in the eddy core were only half of those measured in the Sub-Antarctic Zone waters surrounding the eddy, but similar to those measured in the PFZ, where the eddy originated 27 days prior. These results suggest that, as for physical and chemical tracers, the eddy maintained its biological characteristics from its source waters creating a unique habitat compared to its surroundings.

Plain Language Summary Mesoscale eddies are rotating currents that are everywhere in the ocean. They are typically tens to one or two hundred km across, with lifetimes spanning weeks to months. Mesoscale eddies have a dramatic impact on the patterns of primary production in the open ocean, the transport of heat and salt across oceanic regions, global biogeochemical cycles, and the feeding behavior of marine predators such as pinnipeds, sharks, billfishes, and seabirds. In this study, we used underwater acoustic measurements to evaluate the effects of a Southern Ocean mesoscale eddy on the distribution of deep water micronekton, a diverse group of small animals including fish, crustacea, and squids. We found that the abundance and vertical distribution of micronekton inside the eddy differed from the surrounding waters. Micronekton distribution was instead more similar to where the eddy had originated a month prior to our sampling. Our results suggest that mesoscale eddies can maintain their biological characteristics from their source waters, creating a unique habitat compared to surrounding waters.

1. Introduction

Southern Ocean mesoscale eddies, rotating currents characterized by spatial scales of 10–100 km and lifetimes of weeks to months, are key foraging regions for top marine predators such as pinnipeds (Bailleul et al., 2010; Campagna et al., 2006; Cotté et al., 2015; Della Penna et al., 2015; d'Ovidio et al., 2013; Dragon et al., 2010) and seabirds (Cotté et al., 2007). These animals forage primarily on micronekton, including small fish, cephalopods, crustaceans, and mesozooplankton. Top predators' diving behavior suggests that many of them feed on prey that is located in the mesopelagic zone, between 200 and 1,000 m (Bost et al., 1997; Klages & Bester, 1998; McMahon et al., 2019).

Despite their importance for Southern Ocean ecosystems (Murphy et al., 2016; Subramaniam et al., 2020), little is known about how mesopelagic micronekton are affected by mesoscale eddies. Micronekton are challenging

© 2022. The Authors.

This is an open access article under the terms of the [Creative Commons Attribution-NonCommercial-NoDerivs License](https://creativecommons.org/licenses/by/4.0/), which permits use and distribution in any medium, provided the original work is properly cited, the use is non-commercial and no modifications or adaptations are made.

to observe: they are too small to be tagged with the animal tracking devices used to study top predators and are invisible to our current satellite sensors, which are generally limited to observing the near-surface of the ocean. Current methods to observe mesopelagic micronekton include midwater trawling (Wiebe et al., 1985), optical devices (Kloser et al., 2016), and acoustic techniques (Kloser et al., 2009; Ryan et al., 2009). Furthermore, the distribution of micronekton varies at many temporal and spatial scales. These include the scales spanning diel vertical migration (DVM) behaviors (DVM; Cuvier, 1817; Hays, 2003) to seasonal and interannual variability (Escobar-Flores et al., 2018; Urmy & Horne, 2016). Disentangling this variability in the remote Southern Ocean is further complicated by the logistical challenges of collecting ship-based data in the often harsh conditions of this region.

In recent years, observations of acoustic backscatter have been growing, resulting in the creation of data sets of multifrequency observations from research vessels and ships of opportunity (Kunnath et al., 2021). This suite of observations facilitates an analysis of basin scale patterns in the vertical distribution of mesopelagic organisms (Klevjer et al., 2016) and complements net trawl data in the definition of biogeographical provinces, or bioregions, for mesopelagic organisms (Olivar et al., 2017; Proud et al., 2017; Sutton et al., 2017). Bioregions define the large-scale habitat and areas of ecological interest for marine animals that prey on mesopelagic micronekton (Hindell et al., 2020). Yet, such bioregions do not capture the fine-scale variability that highly mobile predators encounter during foraging trips. This variability is largely influenced by mesoscale (10–100 km) and submesoscale (<10 km) features such as fronts, filaments, and eddies (Bost et al., 2009; Braun et al., 2019; Chapman et al., 2020; Gaube et al., 2018; Tew-Kai et al., 2009) and is central in understanding the role of patchiness in modulating biogeochemical fluxes (Ellwood et al., 2020; Frenger et al., 2018; Moreau et al., 2017; Orselli et al., 2019; Patel et al., 2020; Rohr et al., 2020a, 2020b). An improved understanding of how meso and submesoscales distribute micronekton and mesozooplankton is pivotal for building a comprehensive view of marine ecosystems, from phytoplankton to top predators, including their role in exporting carbon into the deep ocean (Belcher et al., 2019; Davison et al., 2013).

In the North Atlantic, a handful of studies observed how eddies impact the distribution of micronekton using both midwater trawls and acoustic backscatter (Boyd et al., 1986; Craddock et al., 1992; Della Penna & Gaube, 2020; Devine et al., 2021; Godø et al., 2012; Fennell & Rose, 2015). In this region, eddies differed in micronekton abundances, community composition, and patterns in acoustic backscatter from their surrounding waters. A growing number of studies are addressing the distribution of acoustic backscatter in the Southern Ocean, either to relate observed patterns to hydrographic features (Baudena et al., 2021; Béhagle et al., 2017; Escobar-Flores et al., 2018) or to define the boundaries of mesopelagic biogeographies (Proud et al., 2015). However, no published study has explicitly addressed how Southern Ocean mesoscale eddies affect the distribution of acoustic backscatter associated with micronekton.

Here, we combine hydrographic and acoustic measurements to analyze how a Southern Ocean cyclonic eddy modulated acoustic backscatter vertically integrated over the upper 1,200 m, along with its impact on the distribution of deep scattering layers (DSL). First, we highlight the contrasting vertical distributions of acoustic backscatter inside the eddy core with the surrounding waters from the case study of a transect. We relate some of these differences to gradients in the light properties of the water column. Second, we show how integrated acoustic backscatter in the eddy core relates to ambient Sub-Antarctic Zone (SAZ) waters and the waters in the Polar Frontal Zone (PFZ) where the eddy formed. Finally, we discuss how the provenance of the eddy influences the acoustic properties associated with resident micronekton. Specifically, while the eddy core displays acoustic properties that are more similar to its origin, the waters at the eddy periphery display more similarities to the SAZ, suggesting that at the eddy margin mesopelagic communities are mixed with those from the SAZ.

2. Materials and Methods

2.1. Multiplatform Sampling of the Eddy and Its Region

We tracked a cyclonic feature in the Southern Ocean using satellite data: altimetry-derived absolute dynamic topography (ADT) and sea level anomaly (SLA), sea surface temperature (SST), and near-surface chlorophyll (Patel et al., 2019). In particular, we used SLA maps to track the eddy (Figure 1a). Altimetry data were downloaded from the Copernicus CMEMS web portal as daily maps gridded to a nominal spatial resolution of $\frac{1}{4}^\circ$. We first identified the mesoscale feature as a meander in the Sub-Antarctic Front (SAF), which separates the SAZ

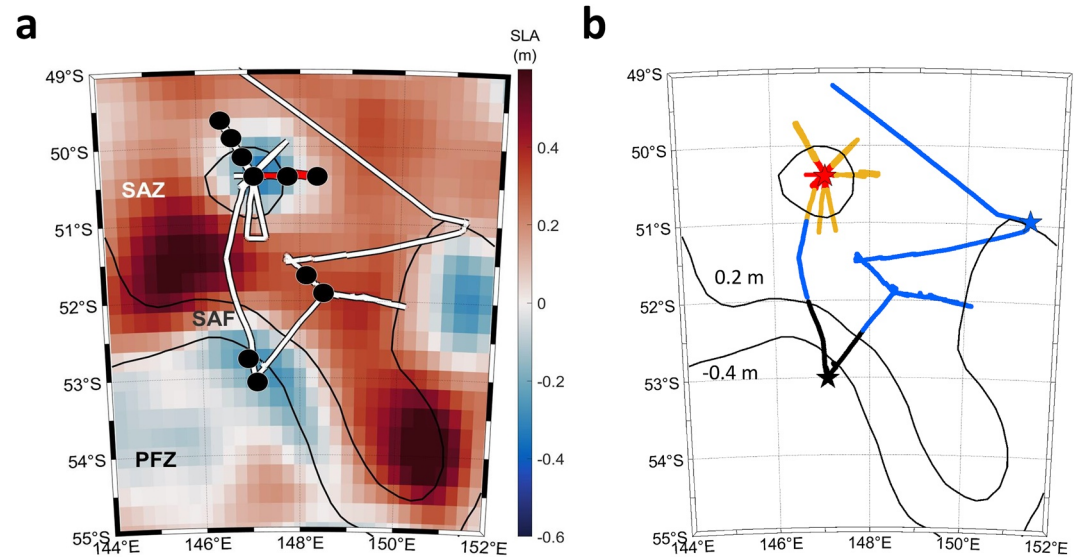


Figure 1. Map of sea level anomaly (SLA, referring to 1 April 2016) for the region of interest (a) and demarcation of different subregions (b). Black contours indicate isolines of absolute dynamic topography (ADT) and identify the eddy and two branches of the Sub-Antarctic Front (SAF) separating the Polar Frontal Zone (PFZ) from the Sub-Antarctic Zone (SAZ). White lines in (a) identify the ship track and black circles the locations of the conductivity, temperature, and depth (CTD) casts. Note that at the scale of this map a few CTD stations are overlapped. The transect shown in Figure 3 corresponds to the part of the ship track marked in red in (a). Colors in (b) indicate the eddy core (red), the eddy periphery (ocher), the PFZ (black), and the SAZ (blue). Stars correspond to the locations of the echograms displayed in Figure S5 in Supporting Information S1.

and the PFZ, on 3 February 2016. On 3 March 2016, the meander detached as a cyclonic eddy and started moving northward onto the SAZ (Patel et al., 2019). The eddy had a diameter of ~ 190 km and was sampled between 30 March and 5 April 2016, during the voyage IN2016_V02 of the Australian *RV Investigator*. We sampled the eddy with a star-shaped pattern of 1,500-m deep conductivity, temperature, and depth (CTD) stations (Figure 1a). After 6 days in the eddy, the *RV Investigator* headed to the PFZ, where the eddy had originated 27 days before the beginning of our sampling (Moreau et al., 2017; Patel et al., 2019). In the PFZ, we conducted two 1,500-m deep CTD stations before the *RV Investigator* headed to Hobart, Tasmania, allowing for further sampling of the SAZ in the vicinity of the eddy. The eddy was reabsorbed by an SAF meander ~ 20 days after we sampled it (Patel et al., 2019).

A total of 18 CTD stations to 1,500 m, complemented with continuous thermosalinograph and inline fluorometer sampling, allowed characterization of the physical and biogeochemical properties of the eddy, its surrounding SAZ waters, and the PFZ. The ensemble of these observations revealed a marked doming of isopycnals as well as anomalies in temperature, oxygen distribution, salinity, chlorophyll-*a*, and nitrates inside the eddy (Moreau et al., 2017; Patel et al., 2019, 2020). Compared to the ambient waters of the SAZ, the eddy was colder (7.55 versus 9.68°C), fresher (34.03 versus 34.54 g/kg), more oxygenated (293.96 versus 276.68 $\mu\text{mol L}^{-1}$), richer in nitrates (21.42 versus 14.17 $\mu\text{mol L}^{-1}$) and poorer in near-surface chlorophyll-*a* (0.39 versus 0.71 $\mu\text{g L}^{-1}$; Figure 2).

The onboard 75 kHz acoustic Doppler current profiler (ADCP) was used to identify the location of the eddy center following Patel et al. (2019) and to discriminate between the eddy core and periphery (in red and ocher, respectively, in Figure 1b). Here, we consider the eddy core as the region within 25 km from the eddy center (red in Figure 1b), where geostrophic velocities near the surface were smaller than 30 cm/s (Patel et al., 2019). We assume all observations within an annulus with radii of 25 and 75 km as belonging to the eddy periphery (ocher in Figure 1b). Contours of ADT were used to separate the measurements from the PFZ (black in Figure 1b) and the SAZ (blue in Figure 1b) following Sokolov and Rintoul (2009), and this classification was confirmed by the distribution of near-surface tracers such as near-surface fluorescence and salinity (Moreau et al., 2017). Here, we use the definition of PFZ used by Trull et al. (2001) which encompasses the entire region between the SAF and the Polar Front.

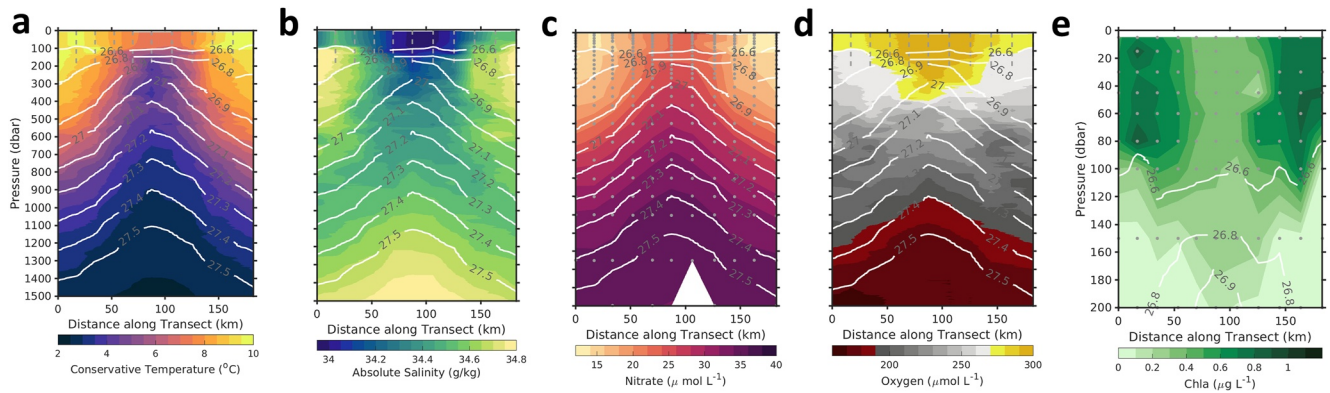


Figure 2. Sections of physical and biogeochemical properties of the sampled eddy. Conductivity, temperature, and depth (CTD) measurements (Figure 1a) revealed that the eddy core was colder (a), fresher (b), richer in nitrate (c), and more oxygenated (d) than the surrounding waters. (e) Observations of chlorophyll-*a* in the epipelagic indicate that the eddy core had lower near-surface chlorophyll-*a* compared to ambient waters and that it was concentrated in the top 100 m. Please note that the y-axis in (e) is different from the other panels. White lines indicate isopycnals.

2.2. EK60 Measurements and Processing

A split-beam scientific echosounder (Simrad EK60, Kongsberg Maritime) was used to measure acoustic volume backscatter (S_v ; dB re 1 m^{-1}) during the entire duration of the trip at the frequency of 18 kHz. Other frequencies were maintained in listening mode, not transmitting, to limit interference with the ADCP, which was essential to map the eddy. Pulse length and period were 2 ms and 0.2 Hz, respectively. The echosounder was calibrated using the standard sphere method before and after the voyage (Demer et al., 2015). We assume no change in the S_v calibration with surface temperature as sound velocity-induced variations cancel out (Bodholt, 2002). Since our study is focused on comparing patterns in the distribution of S_v , any bulk echosounder performance change would not impair our analysis of gradients. We collected >308 hr of acoustic data across the SAZ, PFZ, and the eddy (Table S1 in Supporting Information S1). Day and night observations were defined by comparing the time-stamp associated with each ping with the sunrise and sunset computed from date, longitude, and latitude. Observations collected within 30 min of sunrise and sunset were excluded in the analysis and only retained to plot the echograms (Bianchi & Mislán, 2016).

The star-shaped sampling of the eddy and the irregular vessel speed maintained during the survey to accommodate CTD casts and biogeochemical sampling required a time-based acoustic analysis modified from the standard spatial processing of the IMOS (Integrated Marine Observing System) database which is instead optimized for long straight transects (Kunnath et al., 2021). Raw data of backscattered power were processed using ESP3, an open-source, MATLAB-based package for visualizing and processing acoustics data (Wellington, New Zealand, <https://sourceforge.net/projects/esp3/>; Ladroit et al., 2020). We used observations of temperature and salinity from the CTD casts to calculate the average sound speed and absorption coefficient for the eddy core ($c = 1,474 \text{ m/s}$, $\alpha = 2.99 \text{ dB km}^{-1}$), the eddy periphery ($c = 1,484 \text{ m/s}$, $\alpha = 2.78 \text{ dB km}^{-1}$), the SAZ ($c = 1,487 \text{ m/s}$, $\alpha = 2.71 \text{ dB km}^{-1}$), and the PFZ ($c = 1,472 \text{ m/s}$, $\alpha = 3.01 \text{ dB km}^{-1}$). These coefficients were used to process the acoustic data collected with the echosounder. Spikes caused by bursts of noise from various sources were automatically detected and removed using the ESP3's spike detection algorithm tuned to remove every spike having prominence larger than $10 \text{ dB re } 1 \text{ m}^{-1}$ compared to the average profile. Noise was removed using the ESP3 denoise function, based on De Robertis and Higginbottom (2007), with a noise level threshold of $-110 \text{ dB re } 1 \text{ m}^{-1}$, a signal-to-noise ratio of 1, and a filtering window of 20 m and 20 pings. No corrections were made for nonlinear power responses as outlined by De Robertis et al. (2019) as our results are treated as relative within depth zone indicators. Observations from depths below 1,200 m and shallower than 15 m were excluded from this analysis since the corresponding signal tends to be dominated by noise and backscatter interference. Nautical area scattering coefficients (NASC; $\text{m}^2 \text{ nmi}^{-2}$) were calculated using the equations detailed in MacLennan et al. (2002) integrating over intervals of 5 m and 10 pings, with no threshold on the filtered S_v values for integration. NASC are commonly used in fisheries acoustics to represent the linear increase of fish numbers (biomass) under the assumption that the observed fish has uniform size/weight and acoustic reflectivity. In this study, because we have no accurate information on the size and species composition of the local mesopelagic

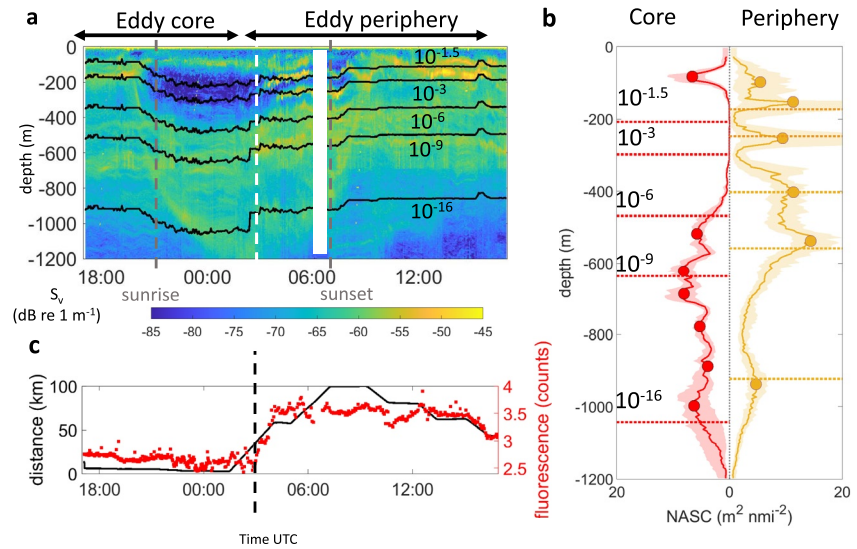


Figure 3. Transition between the eddy core and eddy periphery in acoustic backscatter (a, b) and near-surface fluorescence (c). (a) The echogram shows the transition (white dashed line) between the eddy core and eddy periphery corresponding to the transect indicated in Figure 1a. Gray vertical dashed lines indicate the times of the diel vertical migration (DVM), toward the mesopelagic at $\sim 20:00$ UTC/ $06:00$ local time and up from the mesopelagic at $08:00$ UTC/ $18:00$ local time. White space indicates data that were not retained during quality control. Black contours represent isolines. Differently labeled isolines represent the photosynthetically available radiation (PAR) at a given depth ($\mu\text{E m}^{-2} \text{s}^{-1}$). (b) Average NASC for the observations from the daytime section of the echogram in (a) in the core (red) and at the periphery (ocher) of the eddy. Filled circles along the profiles indicate the position of the detected deep scattering layers (DSL) and dashed lines the corresponding average daytime PAR from (a). Shading indicates the 25th and 75th percentiles over the daytime observations for the time period in (a). As the distance from the eddy center increases (c, black line), the boundary of the eddy core is crossed around 25 km from its center and a sharp gradient in surface fluorescence appears (red dots in c).

micronekton, we use NASC as a proxy of changes in the ecological characteristics of micronekton, in particular of the combined effect of changes in biomass, size, and community composition.

The multibeam EM12 swath mapper, which was constantly operating and synchronized, created a band of interference noise between 400 and 700 m (see e.g., in Figure 3). To test the impact of this interference band on our analysis, we compared NASC in the eddy, its periphery and its origin waters, when including and excluding the 400–700-m depth signal (Figure S1 in Supporting Information S1). Based on this comparison, the inclusion of the interference band did not compromise our analysis, based on comparing observations collected during different times of the same survey.

2.3. ADCP Measurements of Acoustic Backscatter

To mitigate the impact of organisms resonating at a specific frequency, we complemented our acoustic data set with a 75 kHz ADCP. ADCP data were collected for the entire voyage using a 75-kHz narrowband Teledyne RDI Ocean Surveyor. These observations provided estimates of the vertical distribution of horizontal currents down to 750 m that were used to identify the center, the core, and the periphery of the eddy (see Figure 11 in Patel et al., 2019). The ADCP also provided the amplitude of the acoustically backscattered signal from organisms in the water column. While this ADCP was not calibrated to estimate biomass from the backscattering signal, and information about the specific settings of the instrument is not available, it is still possible to extract patterns of uncalibrated backscatter (Gostiaux & van Haren, 2010). We processed the data using the Common Oceanographic Data Access System software processing package (CODAS; Firing, 1995) and then followed the approach described by Picco et al. (2017) to convert the amplitude of backscatter signal into the backscatter coefficient S_v and then into NASC* (uncalibrated NASC) for each 16-m depth bin. We used estimates of sound speed and acoustic absorption for each subregion as detailed in Section 2.1 and average values for factory settings such as the transmit power and system noise constant (transmit power $k_1 = 6.1$ W, system noise constant $k_2 = 2.2$, frequency-dependent constant $k_3 = 1.09 \times 10^5$). The absolute values of acoustic backscatter obtained with this

method are sensitive to these values. However, our analyses looking at the patterns within a voyage are not. Patterns in acoustic intensity obtained from ADCP data have been successfully used to evaluate the timing and velocities of the DVM (Bianchi et al., 2013), validate optical proxies for vertical migration patterns (Behrenfeld et al., 2019), and estimate changes in the abundances of micronekton (Receveur et al., 2020).

2.4. Composites of Acoustic Backscatter Across Subregions

To compare the average distribution of acoustic backscatter in different subregions, we calculated the median daytime profile, 75th and 25th percentiles for each acoustic frequency and for each subregion (SAZ, PFZ, eddy periphery, and eddy core, Figure 1b). We focused on the daytime distribution of acoustic backscatter because vertically migrating organisms tend to occupy the top 200 m of the water column during the night. Therefore, differences in the distribution of DSL are more easily attributable to processes other than DVM during the day.

2.5. Identification of DSL

To analyze the distribution of DSL, we averaged daytime acoustic profiles over given time intervals. The profiles were then smoothed using a moving average with a 15 m span to then identify local maxima defined as a point along a profile more prominent than its two neighboring depths. Only local maxima with a magnitude exceeding $2 \text{ m}^2 \text{ nmi}^{-2}$ that of the neighboring depths were retained as DSL. This threshold was determined as a compromise between being able to discriminate DSL which were obvious to a visual inspection and avoiding false positives due to the noise associated with backscatter profiles. This method is not suited for the analysis of large acoustic data sets, that require more flexible approaches, such as those described by Cade and Benoit-Bird (2014) and Proud et al. (2015). However, for this study, focused on averaged profiles and echograms referring to a few hours or days, this algorithm provided results that corresponded to the visual inspection of echograms.

2.6. Estimates of Underwater Light Levels and Near-Surface Fluorescence

We combined measurements of near-surface photosynthetically available radiation (PAR; $\mu\text{E m}^{-2} \text{ s}^{-1}$) with estimates of light attenuation to assess light levels in the water column. Two PAR sensors (LI-COR LI-190 Quantum Sensors) continuously measured PAR from each side of the *R/V Investigator*. We used the average value of these two measurements to estimate near-surface PAR. Measurements from the starboard and port side never differed $>25 \mu\text{E m}^{-2} \text{ s}^{-1}$.

We used CTD profiles of PAR to estimate light attenuation coefficients. Daytime CTD casts with PAR measurements were obtained as follows: four in the eddy core, four at the periphery, three in the SAZ, and two in the PFZ. Since the light levels that characterize the mesopelagic are below the detection limit of the PAR sensor (Log Quantum Cosine Irradiance Sensor, QCP2300, Biospherical), we estimated a representative coefficient of diffuse light attenuation ($k_d(\text{PAR}); \text{m}^{-1}$) for each CTD cast and averaged for each subregion. Daytime observations of PAR between 50 and 150 m were used to fit a linear relationship between $\log(\text{PAR})$ and depth, and averaged (Figure S2 in Supporting Information S1). The choice of the depth interval 50–150 m was guided by the need to mitigate the impact of varying near-surface plankton (Figure 2e) and the depths where PAR is above the instrument's detection limit (~ 200 m). We conducted a sensitivity test to evaluate how the choice of the depth interval impacted the region-averaged $k_d(\text{PAR})$ estimates. The test showed that, while the values of the attenuation coefficients obtained using different reference depth ranges changed, the relative change between region-averaged $k_d(\text{PAR})$ was robust (Figure S3 in Supporting Information S1). The region-averaged $k_d(\text{PAR})$ data were used to estimate the average profiles of irradiance for each subregion and compared with a Student's t test.

In the transition between subregions, we used uncalibrated measurements of fluorescence of near-surface water to assess surface biological gradients and their impact on light penetration. Near-surface water was sampled through the shipboard flow-through system using a WETStar fluorometer (WS3S-443P, Wetlabs, SeaBird Inc.). As detailed in Moreau et al. (2017), these fluorescence measurements included daily variability caused by nonphotochemical quenching. However, the variability caused by NPQ on shorter time scales, such as those discussed in this study, is an order of magnitude smaller than the gradients we analyzed.

2.7. Historical Acoustics Observations of the Southern Ocean

To provide context for our acoustic observations, we integrated into our study a collection of IMOS acoustic observations collected by research vessels and ships of opportunity (<https://portal.aodn.org.au/>). This data set contains processed acoustic backscatter (S_v) that has been filtered for different types of noise following the guidelines described in Kunnath et al. (2021). From this relatively large data set, we selected only the observations collected at 18, 38, and 70 kHz during the summer-fall months (January-May). We then separated the observations obtained in the SAZ from those collected south of the SAF, in the PFZ. The SAF was defined using the 0.2 m ADT isoline following Sokolov and Rintoul (2009).

3. Results

The vertical distribution of acoustic backscatter was different between the eddy core and the surrounding SAZ waters (Figure 3 and Figure S5 in Supporting Information S1). The example in Figure 3 shows observations of acoustic backscatter sampled from the eddy core to its periphery, and toward ambient SAZ waters. When the vessel moved from the eddy core into the periphery, at about 25 km from the eddy's center (black line in Figure 3c), the distribution of acoustic backscatter changed dramatically (~3:00 a.m. UTC/13:00 local time, white dashed line in Figure 3a and black dashed line in Figure 3c). The depths of several DSL present both inside the eddy core and at the periphery were different in these two subregions (Figures 3a and 3b). The deepest scattering layer in the core shoaled from ~1,000 m to 900 m as the vessel left the eddy core, while the lower limit of the nonmigrating DSL shoaled from ~500 to ~420 m and from ~620 m to <550 m. Furthermore, some scattering layers, such as those at 200–300 m, were observed immediately outside of the eddy core, but not inside.

The general shift of most DSL toward shallower depths matched the uplift of isolines (black contours in Figure 3a and dashed lines in Figure 3b). This shift cannot be attributed to the DVM of acoustic targets as it occurred in the middle of the day, >3 hr after and prior to sunrise and sunset, respectively. Changes in light levels were affected by minor changes in surface PAR and changes in light attenuation coefficients which in turn were collocated with changes in near-surface fluorescence (higher outside the eddy, Figure 3c). The clearest waters were in the eddy core and the PFZ. The highest attenuation coefficients were in the SAZ. Average light attenuation coefficients in the eddy core were significantly lower than those from surrounding SAZ waters (0.0402 versus 0.0513 m^{-1} ; $p < 0.05$), yet not significantly different from the origin PFZ waters (0.0333 m^{-1} ; p -value = 0.27) and the eddy periphery (0.0446 m^{-1} ; p -value = 0.07; Figure S4 in Supporting Information S1).

On average, DSL in the eddy core were less reflective compared to the SAZ (Figure 4a, Figure S5 in Supporting Information S1). The median integrated daytime NASC at 18 kHz inside the core of the eddy was ~50% of the NASC in the surrounding waters of the SAZ (847 $\text{m}^2 \text{nmi}^{-2}$ versus 1875 $\text{m}^2 \text{nmi}^{-2}$; Figure 4c and Figure S1 in Supporting Information S1). Daytime integrated values of NASC in the PFZ (757 $\text{m}^2 \text{nmi}^{-2}$) were also as low as inside the eddy core and noticeably smaller than the SAZ (Figure 4c). This coherence between the eddy core and the PFZ where it formed was most evident in the upper mesopelagic where the average integrated NASC was 122 $\text{m}^2 \text{nmi}^{-2}$ in the eddy core, 204 $\text{m}^2 \text{nmi}^{-2}$ in the PFZ, and 817 $\text{m}^2 \text{nmi}^{-2}$ in the SAZ (Figure S1 and Table S2 in Supporting Information S1). By contrast in the epipelagic and lower mesopelagic (600–1,200 m), eddy core average integrated NASC was closer to the average values measured in the SAZ (Figure S1 and Table S2 in Supporting Information S1). Differences between integrated NASC values between the eddy core and the SAZ and the eddy core and the PFZ were statistically significant with p -values $< 10^{-10}$ and $p = 0.03$, respectively. Acoustic backscatter at 75 kHz from the uncalibrated ADCP (NASC*) revealed a similar pattern, with stronger acoustic backscatter in the SAZ compared to the eddy core and the PFZ (Figures 4b and 4d) although displaying different peaks.

Historical 18, 38, and 70 kHz data of acoustic backscatter from the SAZ and PFZ showed similar relative differences to those observed during our sampling. Integrated NASC values in the SAZ were more than three times higher than in the PFZ (Figure 5). Median profiles of NASC calculated for these three frequencies showed that, for all frequencies, backscattering in the SAZ was more intense compared to the PFZ across all depths (Figure S6 in Supporting Information S1).

NASC differences in the mesopelagic between the eddy core and those in the PFZ were less than half of the differences between the eddy core and the SAZ (Figure 6). For example, at 400 m, the difference between the eddy core and the SAZ was $-10 \text{ m}^2 \text{nmi}^{-2}$ whereas the difference between the eddy core and the PFZ was

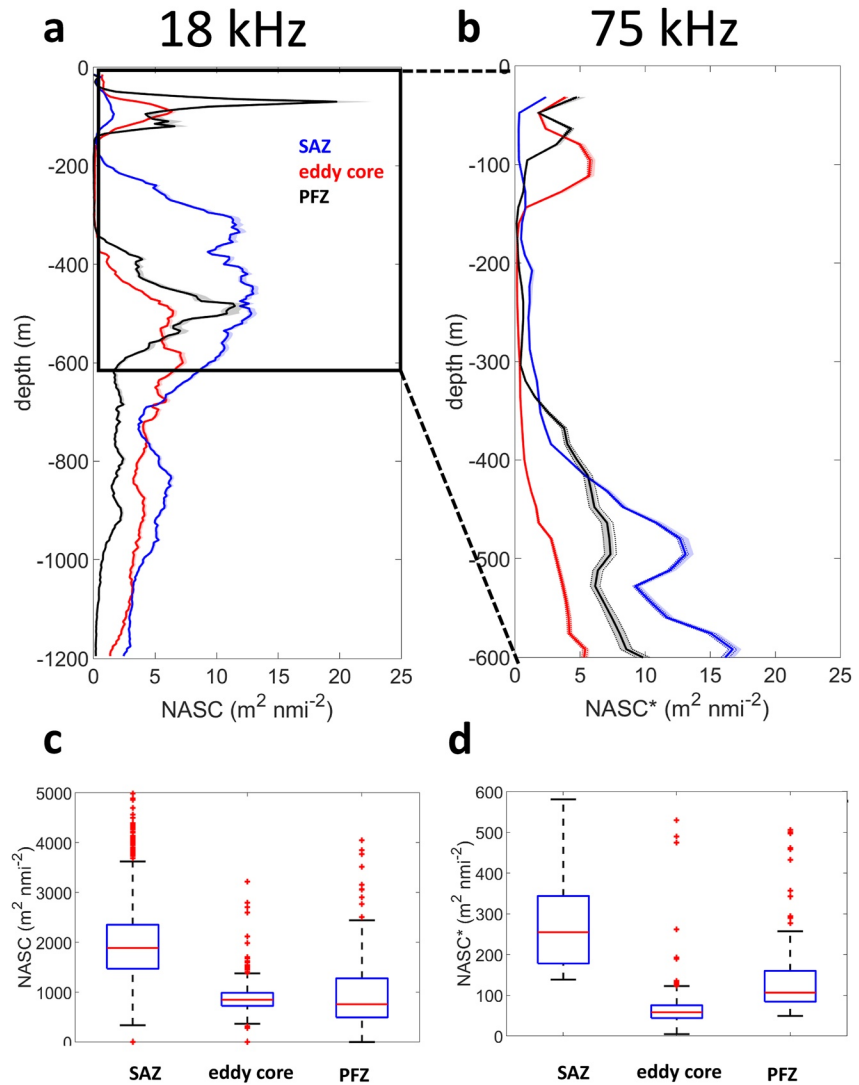


Figure 4. Vertical distribution of median daytime acoustic backscatter (a, b) and integrated daytime NASC/NASC* (c, d) at 18 kHz (a, c) and 75 kHz (b, d). Solid lines in (a) and (b) indicate the median daytime NASC/NASC* of all measurements collected in the Sub-Antarctic Zone (SAZ; blue), the eddy core (red), and the Polar Frontal Zone (PFZ; black). Shading indicates the 25th and 75th percentiles divided by the square root of the number of daytime profiles available (see Table S1 in Supporting Information S1). Values in (c) and (d) were integrated over the top 1,200 m (c) and 600 m (d). Note that the y-axis in (a) and (b) are different because of the different attenuation of sound at 18 and 75 kHz. The black box in (a) indicates the y-axis in (b).

$-2 \text{ m}^2 \text{ nmi}^{-2}$. NASC from the eddy periphery was, on average, intermediate between the SAZ and the eddy core (Figure 6a). Conversely, NASC values measured at the eddy periphery were on average of larger magnitude than the PFZ (positive anomalies in Figure 6b) at all depths below 100 m and above 650 m. These patterns were most evident in the upper mesopelagic. In the epipelagic high values of average daytime NASC detected in the PFZ, constrained in the top 100 m (Figure 6; Table S2 in Supporting Information S1), created the strongest anomalies for both the eddy core and the eddy periphery ($\Delta \text{NASC} \sim -15 \text{ m}^2 \text{ nmi}^{-2}$). Below 650 m anomalies for both the average eddy core and periphery observations were of small magnitude compared to those measured in the upper mesopelagic, yet they showed generally larger differences between the eddy core/periphery and the PFZ compared to the SAZ.

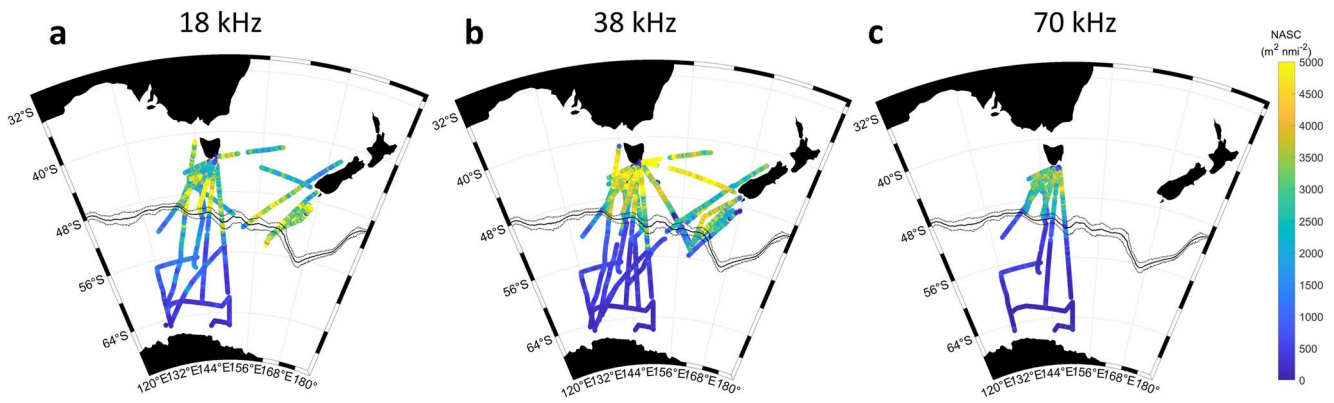


Figure 5. Patterns of integrated acoustic backscatter over the upper 600 m at 18 kHz (a), 38 kHz (b), and 70 kHz (c) measured between January and May in the Sub-Antarctic Zone (SAZ) and Polar Frontal Zone (PFZ). The black solid line indicates the average locations of the Sub-Antarctic Front (SAF), separating the SAZ (north) and the PFZ (south), at the times of the observations. Dashed lines indicate the position of the front \pm one standard deviation.

4. Discussion and Conclusions

We examined the daytime distribution of acoustic backscatter inside a Southern Ocean cyclonic eddy and compared it against ambient (SAZ) and origin (PFZ) waters. Our major findings were as follows:

1. The vertical distribution of acoustic backscatter at 18 and 75 kHz inside the eddy core was different from the ambient waters of the SAZ, even a month after eddy formation (Figures 3 and 4). Because we have focused on daytime measurements, none of these patterns can be attributed to the DVM of acoustic targets.
2. Sharp changes in acoustic backscatter co-occurred with changes in light levels and light penetration, which in turn matched near-surface fluorescence variability (Figure 3).
3. The average water-column integrated NASC at 18 kHz inside the eddy core ($847 \text{ m}^2 \text{ nmi}^{-2}$) was similar to that of the PFZ ($757 \text{ m}^2 \text{ nmi}^{-2}$) but 50% lower than the average NASC in the SAZ ($\sim 2,000 \text{ m}^2 \text{ nmi}^{-2}$, Figure 4c; Table S2 in Supporting Information S1).
4. Records of acoustic backscatter at 18, 38, and 70 kHz from the IMOS historical data set indicate that the PFZ-SAZ differences observed during our cruise are a consistent pattern in this sector of the Southern Ocean (Figure 5).

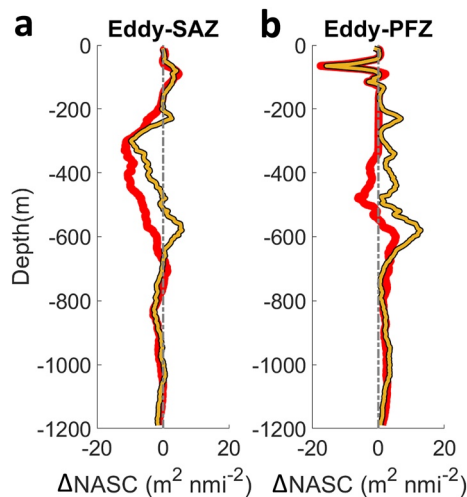


Figure 6. Differences between the median (calculated over all the daytime observations) 18 kHz acoustic backscatter in selected areas of the eddy (core in the red line, periphery in other), the Sub-Antarctic Zone (SAZ, a), and the Polar Frontal Zone (PFZ, b) as a function of depth.

Inside the eddy, light penetrated deeper into the water column because of low chlorophyll-*a* in the upper 100 m and optically clearer waters (Figure 3c). We estimated very low light attenuation coefficients typical of the Southern Ocean during fall and winter (Nelson & Smith, 1991; Son & Wang, 2015). Although we only had two CTD casts in the PFZ, light attenuation coefficients there were not statistically different (p -value = 0.27) from the eddy core, suggesting that the eddy maintained the optical properties of its origin. On the other hand, light attenuation coefficients in the eddy core were significantly lower than in the SAZ (p -value < 0.05). As observed in other basins (Della Penna & Gaube, 2020), the horizontal gradients in the vertical distribution of acoustic backscatter were sharp and matched the gradients in near-surface fluorescence at the transition between the core and the periphery. As suggested in previous studies (Aksnes et al., 2017; Røstad et al., 2016), light was a key driver of the variability in the acoustic backscatter vertical distribution.

Light penetration depends not only on attenuation by water, chlorophyll, and particles, but also on surface irradiance. We collected acoustic observations over 10 days, during which the atmospheric conditions were not constant. Omand et al. (2021) discovered that, even in relatively constant cloudy conditions, the DSL depth can oscillate by up to 60 m due to high frequency (< 1 hr) changes in the distribution of isolumes caused by relatively small

differences in cloud cover. This trend is also evident in our results where the isolines oscillated during the day in response to changes in cloud cover and solar angle (Figure 3 and Figure S7 in Supporting Information S1). Southern Ocean cyclones, on average, cause a decline in overlying cloud fraction and atmospheric water content, which we expect would be reflected in increased ocean surface PAR (Frenger et al., 2013). This could explain the deeper DSL in the eddy, but surface PAR in this eddy core was lower compared to surrounding SAZ waters (Figure S8 in Supporting Information S1). Therefore, changes in depth of the DSL were not linked to changes in cloud cover and surface irradiance caused by the presence of the eddy.

The eddy core retained the vertical distribution of acoustic properties from its origin waters and also the signature of integrated backscatter in the mesopelagic. This suggests that micronekton were transported from the PFZ >200 km north in the SAZ, likely resulting from eddy trapping (Early et al., 2011). The eddy in this study was rotating on average at ~40 km/day and moved laterally between 1.5 and 6.6 km/day (1.7 km/day at the time of sampling, and maxima of 6.6 km/day when detaching from the meander; Patel et al., 2019). The resulting speed ratio of rotation to translation (>1 indicates nonlinearity; Chelton et al., 2011) was >5 for the entire lifetime of the eddy, suggesting that this eddy was highly nonlinear and likely contained a core of trapped water. This parcel of water, trapped in the eddy, was observed to extend beyond 1,300 m (Figure S9 in Supporting Information S1). This suggests that vertically migrating layers spent their time in the eddy and did not leave during the day. Our results, however, suggest that differences in mesopelagic NASC between the eddy core and the PFZ were smaller compared to those between core and SAZ down to ~650–700 m. This suggests that the eddy trapped mesopelagic communities only at depths with a strong nonlinearity.

Eddy trapping has significant consequences for the transport of salt and heat across the Antarctic Circumpolar Current (Patel et al., 2019), impacts the distribution of primary producers (Dawson et al., 2018; Frenger et al., 2018) and weather (Frenger et al., 2013), and regulates the exchanges of carbon crucial for climate (Dufour et al., 2015; Moreau et al., 2017). Our results show that eddy trapping also impacts mesopelagic micronekton. It is difficult to evaluate whether micronekton themselves were trapped and transported or if it was their zooplanktonic prey that was transported and the micronekton responded to a change in prey. What is clear is that the eddy presented a unique environment compared to the SAZ waters, similar to what past studies have found in other regions (Boyd et al., 1986; Craddock et al., 1992). Yet, without complementary observations of zooplankton and micronekton community composition in the epipelagic and mesopelagic, it is not possible to provide a definitive answer to whether the fish were transported or not. However, to initiate movement and, e.g., leave the eddy core, it is likely that micronekton would be responding to a stimulus, such as a gradient in temperature, pressure, or light (Franks, 1992). From the inner core of a mesoscale eddy, the closest horizontal gradients in such properties are tens of kilometers away requiring a mesopelagic fish to be able to perceive a gradient on scales that are 4 orders of magnitudes larger than their body size (i.e., few centimeters). In addition to this, horizontal gradients associated to mesoscale features are generally orders of magnitude weaker than the vertical ones that vertically migrating mesopelagic fish interact with during the DVM. Furthermore, studies focused on trawl and predator avoidance suggest that most mesopelagic micronekton are generally lethargic when not vertically migrating or actively escaping from a threat (Barham, 1966; Craddock et al., 1992; Kaartvedt et al., 2009, 2012). These lines of evidence suggest that micronekton could have been trapped within the eddy core with their prey.

Our results also indicate that, while the eddy core preserved many of the acoustic properties of the PFZ, the eddy periphery was more similar to the SAZ (Figure 6). We can interpret this pattern as an indicator of lateral exchanges and mixing of water parcels, and the organisms they contained, between the SAZ and the periphery of the eddy as suggested also in previous studies in the North Atlantic (Boyd et al., 1986). This result is supported by the analysis of water mass properties based on CTD data collected during the same voyage (Moreau et al., 2017) and by the overall distribution of biogeochemical tracers (Patel et al., 2020) including oxygen (Figure S10 in Supporting Information S1). These findings are consistent with the theoretical results about eddy trapping by Early et al. (2011), who highlighted that while eddy core waters can be isolated for a significant part of an eddy lifetime, the peripheries of eddies regularly exchange water masses with the surroundings.

Attribution of species and biomass to the mesopelagic acoustic data is normally done with a combination of sampling devices including nets, and optical and acoustic probes (Davison et al., 2015; Fernandes et al., 2002; Kloser et al., 2016). This research would have been significantly enhanced with a direct sampling of the scattering layers and is part of ongoing infrastructure and research efforts. Inferring acoustic community composition in the mesopelagic zone improves also when extra frequencies are used (Béhagle et al., 2017; Trenkel & Berger, 2013).

The strong difference between the SAZ and PFZ observed during this study, both in terms of integrated NASC, and vertical distribution of backscattering at two frequencies, was corroborated by the historical data from the IMOS database at three frequencies, that consistently showed less acoustic backscatter in the PFZ compared to the SAZ (Figure 5). This was also demonstrated in other studies that reported a general decrease in acoustic backscatter with increased latitude (Chawarski et al., 2022; Dornan et al., 2019; Escobar-Flores et al., 2018, 2020). These changes in acoustic backscatter were not always correlated to changes in fish biomass. Dornan et al. (2019), who analyzed changes in acoustic backscatter between 52°S and 60°S, showed that changes in animal size and community composition were responsible for the poleward decrease in backscatter. During IN2016_V02, we did not carry out any midwater trawling, and, therefore, we cannot discriminate whether the patterns we identified in backscatter are a result of changes in fish abundance, size, or community composition. What is clear is that the cyclonic eddy trapped, preserved, and transported organisms having acoustic properties of PFZ waters across warmer, more productive SAZ waters for weeks.

Differences in the horizontal and vertical distribution of mesopelagic micronekton can have important consequences for upper trophic levels. The organisms inhabiting the DSL we detected typically include myctophids, squids, and swarming euphausiids (Escobar-Flores et al., 2020). These animals constitute the prey of a variety of marine megafauna, including seabirds, penguins, and marine mammals (Cherel et al., 2010; McMahon et al., 2019; Watanuki & Thiebot, 2018). For these diving predators, the horizontal patchiness of their prey field is an important driver of their foraging strategies. Differences in micronekton composition or abundance can underpin their interactions with the prey fields which are in turn set by the dynamics associated with mesoscale eddies. Furthermore, the differences in the vertical distribution of DSL are likely to have an impact on the accessibility of the prey to diving predators. This difference might be particularly dramatic for air-breathing animals such as seabirds and marine mammals whose foraging time underwater is limited by the need to breathe at the surface (Guinet et al., 2014; Jaud et al., 2012; O'Toole et al., 2017), but also to fish whose thermal niche can limit the vertical extent of their diving behavior (Arostegui et al., 2022; Braun et al., 2019; Gaube et al., 2018). In general, for air-breathing predators or fish whose thermal niche is constrained, the metabolic cost associated with getting the same amount of energy if the prey is located deeper in the water column (and therefore potentially in colder water) will be higher. These costs have the potential to result in cyclonic eddies, like the one we sampled, being a less profitable region for foraging.

Eddy prevalence, as quantified by eddy kinetic energy, is increasing in the Southern Ocean (Martínez-Moreno et al., 2021). This has potentially strong implications for the meridional fluxes of heat, salt, carbon, and nutrients (Moreau et al., 2017; Patel et al., 2019, 2020), especially for eddy hot-spots in the Southern Ocean which preferentially generate either cyclones (as our study area) or anticyclones (Frenger et al., 2015). This work extends these previous findings suggesting a potential impact on micronekton and the Southern Ocean predators that rely on them.

Acknowledgments

We would like to thank the Captain, the crew, and the technicians and scientists onboard of the IN2016_V02 voyage. This study has been conducted using E.U. Copernicus Marine Service Information (CMEMS). This research was supported under Australian Research Council's Special Research Initiative for Antarctic Gateway Partnership (Project ID SR140300001), by the Australian Research Council Discovery Grant DP160102870, the ARC Centre of Excellence for Climate System Science (CE1101028), and ship time from Australia's Marine National Facility. In addition, Joan Llort was supported by the European Union's Horizon 2020 Research and Innovation Programme under the Marie Skłodowska-Curie Grant Agreement 754433. Open access publishing facilitated by The University of Auckland, as part of the Wiley - The University of Auckland agreement via the Council of Australian University Librarians.

Data Availability Statement

All data from the underway system, the CTD, and the echosounder from the IN2016_V02 voyage are available at https://www.marine.csiro.au/data/trawler/survey_details.cfm?survey=IN2016_V02. These data sets are made available under a Creative Commons Attribution 4.0 International Licence. We acknowledge the use of the CSIRO Marine National Facility, <https://ror.org/01mae9353> in undertaking this research. The historical IMOS observations can be extracted from the webportal: <https://portal.aodn.org.au/search>. A complete lists of the URLs for all the IMOS data used in this study can be found in the Supporting Information (ST3, ST4, ST5). Data were sourced from Australia's Integrated Marine Observing System (IMOS)—IMOS is enabled by the National Collaborative Research Infrastructure Strategy (NCRIS). We would like to thank four anonymous reviewers for their constructive comments.

References

- Aksnes, D. L., Røstad, A., Kaartvedt, S., Martinez, U., Duarte, C. M., & Irigoien, X. (2017). Light penetration structures the deep acoustic scattering layers in the global ocean. *Science Advances*, 3(5), e1602468. <https://doi.org/10.1126/sciadv.1602468>
- Arostegui, M. C., Gaube, P., Woodworth-Jefcoats, P. A., Kobayashi, D. R., & Braun, C. D. (2022). Anticyclonic eddies aggregate pelagic predators in a subtropical gyre. *Nature*, 609, 535–540. <https://doi.org/10.1038/s41586-022-05162-6>
- Bailleul, F., Cotté, C., & Guinet, C. (2010). Mesoscale eddies as foraging area of a deep-diving predator, the southern elephant seal. *Marine Ecology Progress Series*, 408, 251–264. <https://doi.org/10.3354/meps08560>

- Barham, E. G. (1966). Deep scattering layer migration and composition: Observations from a diving saucer. *Science*, *151*(3716), 1399–1403. <https://doi.org/10.1126/science.151.3716.1399>
- Baudena, A., Ser-Giacomi, E., D'Onofrio, D., Capet, X., Cotté, C., Cherel, Y., & D'Ovidio, F. (2021). Fine-scale structures as spots of increased fish concentration in the open ocean. *Scientific Reports*, *11*(1), 15805. <https://doi.org/10.1038/s41598-021-94368-1>
- Béghagie, N., Cotté, C., Lebourges-Dhaussy, A., Roudaut, G., Duhamel, G., Brehmer, P., et al. (2017). Acoustic distribution of discriminated micronektonic organisms from a bi-frequency processing: The case study of eastern Kerguelen oceanic waters. *Progress in Oceanography*, *156*, 276–289. <https://doi.org/10.1016/j.pocean.2017.06.004>
- Behrenfeld, M. J., Gaube, P., Della Penna, A., O'Malley, R. T., Burt, W. J., Hu, Y., et al. (2019). Global satellite-observed daily vertical migrations of ocean animals. *Nature*, *576*(7786), 257–261. <https://doi.org/10.1038/s41586-019-1796-9>
- Belcher, A., Saunders, R. A., & Tarling, G. A. (2019). Respiration rates and active carbon flux of mesopelagic fishes (Family Myctophidae) in the Scotia Sea, Southern Ocean. *Marine Ecology Progress Series*, *610*, 149–162. <https://doi.org/10.3354/meps12861>
- Bianchi, D., & Mislán, K. A. S. (2016). Global patterns of diel vertical migration times and velocities from acoustic data. *Limnology & Oceanography*, *61*(1), 353–364. <https://doi.org/10.1002/lno.10219>
- Bianchi, D., Stock, C., Galbraith, E. D., & Sarmiento, J. L. (2013). Diel vertical migration: Ecological controls and impacts on the biological pump in a one-dimensional ocean model. *Global Biogeochemical Cycles*, *27*, 478–491. <https://doi.org/10.1002/gbc.20031>
- Bodholt, H. (2002). The effect of water temperature and salinity on echo sounder measurements. In *ICES Symposium on Acoustics in Fisheries* (pp. 1–7).
- Bost, C. A., Cotté, C., Bailluel, F., Cherel, Y., Charrassin, J. B., Guinet, C., et al. (2009). The importance of oceanographic fronts to marine birds and mammals of the Southern Oceans. *Journal of Marine Systems*, *78*(3), 363–376. <https://doi.org/10.1016/j.jmarsys.2008.11.022>
- Bost, C. A., Georges, J. Y., Guinet, C., Cherel, Y., Pütz, K., Charrassin, J. B., et al. (1997). Foraging habitat and food intake of satellite-tracked king penguins during the austral summer at Crozet Archipelago. *Marine Ecology Progress Series*, *150*, 21–33. <https://doi.org/10.3354/meps150021>
- Boyd, S. H., Wiebe, P. H., Backus, R. H., Craddock, J. E., & Daher, M. A. (1986). Biomass of the micronekton in Gulf Stream ring 82-B and environs: Changes with time. *Deep Sea Research, Part A: Oceanographic Research Papers*, *33*(11–12), 1885–1905. [https://doi.org/10.1016/0198-0149\(86\)90084-1](https://doi.org/10.1016/0198-0149(86)90084-1)
- Braun, C. D., Gaube, P., Sinclair-Taylor, T. H., Skomal, G. B., & Thorrold, S. R. (2019). Mesoscale eddies release pelagic sharks from thermal constraints to foraging in the ocean twilight zone. *Proceedings of the National Academy of Sciences of the United States of America*, *116*(35), 17187–17192. <https://doi.org/10.1073/pnas.1903067116>
- Cade, D. E., & Benoit-Bird, K. J. (2014). An automatic and quantitative approach to the detection and tracking of acoustic scattering layers. *Limnology and Oceanography: Methods*, *12*(11), 742–756. <https://doi.org/10.4319/lom.2014.12.742>
- Campagna, C., Piola, A. R., Marin, M. R., Lewis, M., & Fernández, T. (2006). Southern elephant seal trajectories, fronts and eddies in the Brazil/Malvinas confluence. *Deep Sea Research Part I: Oceanographic Research Papers*, *53*(12), 1907–1924. <https://doi.org/10.1016/j.dsr.2006.08.015>
- Chapman, C. C., Lea, M. A., Meyer, A., Sallée, J. B., & Hindell, M. (2020). Defining Southern Ocean fronts and their influence on biological and physical processes in a changing climate. *Nature Climate Change*, *10*, 209–219. <https://doi.org/10.1038/s41558-020-0705-4>
- Chawarski, J., Klevjer, T. A., Coté, D., & Geoffroy, M. (2022). Evidence of temperature control on mesopelagic fish and zooplankton communities at high latitudes. *Frontiers in Marine Science*, *9*, 917985. <https://doi.org/10.3389/fmars.2022.917985>
- Chelton, D. B., Schlax, M. G., & Samelson, R. M. (2011). Global observations of nonlinear mesoscale eddies. *Progress in Oceanography*, *91*(2), 167–216. <https://doi.org/10.1016/j.pocean.2011.01.002>
- Cherel, Y., Fontaine, C., Richard, P., & Labat, J. P. (2010). Isotopic niches and trophic levels of myctophid fishes and their predators in the Southern Ocean. *Limnology & Oceanography*, *55*(1), 324–332. <https://doi.org/10.4319/lno.2010.55.1.0324>
- Cotté, C., d'Ovidio, F., Dragon, A. C., Guinet, C., & Lévy, M. (2015). Flexible preference of southern elephant seals for distinct mesoscale features within the Antarctic Circumpolar Current. *Progress in Oceanography*, *131*, 46–58. <https://doi.org/10.1016/j.pocean.2014.11.011>
- Cotté, C., Park, Y. H., Guinet, C., & Bost, C. A. (2007). Movements of foraging king penguins through marine mesoscale eddies. *Proceedings of the Royal Society B: Biological Sciences*, *274*(1624), 2385–2391. <https://doi.org/10.1098/rspb.2007.0775>
- Craddock, J. E., Backus, R. H., & Daher, M. A. (1992). Vertical distribution and species composition of midwater fishes in warm-core Gulf Stream meander/ring 82-H. *Deep Sea Research, Part A: Oceanographic Research Papers*, *39*, S203–S218. [https://doi.org/10.1016/S0198-0149\(11\)80012-9](https://doi.org/10.1016/S0198-0149(11)80012-9)
- Cuvier, G. (1817). *Le Règne Animal distribué d'après son Organisation pour à l'Histoire Naturelle des Animaux et d'Introduction à l'Anatomie Compare* (Deterville).
- Davison, P. C., Checkley, D. M., & Koslow, J. A., & Barlow, J. (2013). Carbon export mediated by mesopelagic fishes in the northeast Pacific Ocean. *Progress in Oceanography*, *116*, 14–30. <https://doi.org/10.1016/j.pocean.2013.05.013>
- Davison, P. C., Koslow, J. A., & Kloser, R. J. (2015). Acoustic biomass estimation of mesopelagic fish: Backscattering from individuals, populations, and communities. *ICES Journal of Marine Science*, *72*(5), 1413–1424. <https://doi.org/10.1093/icesjms/fsv023>
- Dawson, H. R., Strutton, P. G., & Gaube, P. (2018). The unusual surface chlorophyll signatures of Southern Ocean eddies. *Journal of Geophysical Research: Oceans*, *123*, 6053–6069. <https://doi.org/10.1029/2017JC013628>
- Della Penna, A., De Monte, S., Kestenare, E., Guinet, C., & d'Ovidio, F. (2015). Quasi-planktonic behavior of foraging top marine predators. *Scientific Reports*, *5*(1), 18063. <https://doi.org/10.1038/srep18063>
- Della Penna, A., & Gaube, P. (2020). Mesoscale eddies structure mesopelagic communities. *Frontiers in Marine Science*, *7*, 454. <https://doi.org/10.3389/fmars.2020.00454>
- Demer, D. A., Berger, L., Bernasconi, M., Bethke, E., Boswell, K., Chu, D., et al. (2015). Calibration of acoustic instruments. *ICES Cooperative Research Report No. 326* (p. 133). <https://doi.org/10.25607/OBP-185>
- De Robertis, A., Bassett, C., Andersen, L. N., Wangen, I., Furnish, S., & Levine, M. (2019). Amplifier linearity accounts for discrepancies in echo-integration measurements from two widely used echosounders. *ICES Journal of Marine Science*, *76*(6), 1882–1892. <https://doi.org/10.1093/icesjms/fsz040>
- De Robertis, A., & Higginbottom, I. (2007). A post-processing technique to estimate the signal-to-noise ratio and remove echosounder background noise. *ICES Journal of Marine Science*, *64*(6), 1282–1291. <https://doi.org/10.1093/icesjms/fsm112>
- Devine, B., Fennell, S., Themelis, D., & Fisher, J. A. (2021). Influence of anticyclonic, warm-core eddies on mesopelagic fish assemblages in the Northwest Atlantic Ocean. *Deep Sea Research Part I: Oceanographic Research Papers*, *173*, 103555. <https://doi.org/10.1016/j.dsr.2021.103555>
- Dornan, T., Fielding, S., Saunders, R. A., & Genner, M. J. (2019). Swimbladder morphology masks Southern Ocean mesopelagic fish biomass. *Proceedings of the Royal Society B*, *286*(1903), 20190353. <https://doi.org/10.1098/rspb.2019.0353>

- d'Ovidio, F., De Monte, S., Della Penna, A., Cotté, C., & Guinet, C. (2013). Ecological implications of eddy retention in the open ocean: A Lagrangian approach. *Journal of Physics A: Mathematical and Theoretical*, *46*(25), 254023. <https://doi.org/10.1088/1751-8113/46/25/254023>
- Dragon, A. C., Monestiez, P., Bar-Hen, A., & Guinet, C. (2010). Linking foraging behaviour to physical oceanographic structures: Southern elephant seals and mesoscale eddies east of Kerguelen Islands. *Progress in Oceanography*, *87*(1–4), 61–71. <https://doi.org/10.1016/j.pocan.2010.09.025>
- Dufour, C. O., Griffies, S. M., de Souza, G. F., Frenger, I., Morrison, A. K., Palter, J. B., & Slater, R. D. (2015). Role of mesoscale eddies in cross-frontal transport of heat and biogeochemical tracers in the Southern Ocean. *Journal of Physical Oceanography*, *45*(12), 3057–3081. <https://doi.org/10.1175/JPO-D-14-0240.1>
- Early, J. J., Samelson, R. M., & Chelton, D. B. (2011). The evolution and propagation of quasigeostrophic ocean eddies. *Journal of Physical Oceanography*, *41*(8), 1535–1555. <https://doi.org/10.1175/2011JPO4601.1>
- Ellwood, M. J., Strzepek, R. F., Strutton, P. G., Trull, T. W., Fourquez, M., & Boyd, P. W. (2020). Distinct iron cycling in a Southern Ocean eddy. *Nature Communications*, *11*(1), 825. <https://doi.org/10.1038/s41467-020-14464-0>
- Escobar-Flores, P. C., Driscoll, R. L., & Montgomery, J. C. (2018). Spatial and temporal distribution patterns of acoustic backscatter in the New Zealand sector of the Southern Ocean. *Marine Ecology Progress Series*, *592*, 19–35. <https://doi.org/10.3354/meps12489>
- Escobar-Flores, P. C., O'Driscoll, R. L., Montgomery, J. C., Ladroit, Y., & Jendersie, S. (2020). Estimates of density of mesopelagic fish in the Southern Ocean derived from bulk acoustic data collected by ships of opportunity. *Polar Biology*, *43*(1), 43–61. <https://doi.org/10.1007/s00300-019-02611-3>
- Fennell, S., & Rose, G. (2015). Oceanographic influences on deep scattering layers across the North Atlantic. *Deep Sea Research Part I: Oceanographic Research Papers*, *105*, 132–141. <https://doi.org/10.1016/j.dsr.2015.09.002>
- Fernandes, P. G., Gerlotto, F., Holliday, D. V., Nakken, O., & Simmonds, E. J. (2002). *Acoustic applications in fisheries science: The ICES contribution*. ICES.
- Firing, E. (1995). *Processing ADCP data with the CODAS software system version 3.1*. Joint Institute for Marine and Atmospheric Research, University of Hawaii & National Oceanographic Data Center.
- Franks, P. J. (1992). Sink or swim: Accumulation of biomass at fronts. *Marine Ecology Progress Series*, *82*(1), 1–12. <https://doi.org/10.3354/meps082001>
- Frenger, I., Gruber, N., Knutti, R., & Münnich, M. (2013). Imprint of Southern Ocean eddies on winds, clouds and rainfall. *Nature Geoscience*, *6*(8), 608–612. <https://doi.org/10.1038/ngeo1863>
- Frenger, I., Münnich, M., & Gruber, N. (2018). Imprint of Southern Ocean eddies on chlorophyll. *Biogeosciences*, *15*, 4781–4798. <https://doi.org/10.5194/bg-15-4781-2018>
- Frenger, I., Münnich, M., Gruber, N., & Knutti, R. (2015). Southern Ocean eddy phenomenology. *Journal of Geophysical Research: Oceans*, *120*, 7413–7449. <https://doi.org/10.1002/2015JC011047>
- Gaube, P., Braun, C. D., Lawson, G. L., McGillicuddy, D. J., Della Penna, A., Skomal, G. B., et al. (2018). Mesoscale eddies influence the movements of mature female white sharks in the Gulf Stream and Sargasso Sea. *Scientific Reports*, *8*(1), 7363. <https://doi.org/10.1038/s41598-018-25565-8>
- Godó, O. R., Samuelsen, A., Macaulay, G. J., Patel, R., Hjøllø, S. S., Horne, J., & Johannessen, J. A. (2012). Mesoscale eddies are oases for higher trophic marine life. *PLoS One*, *7*(1), e30161. <https://doi.org/10.1371/journal.pone.0030161>
- Gostiaux, L., & van Haren, H. (2010). Extracting meaningful information from uncalibrated backscattered echo intensity data. *Journal of Atmospheric and Oceanic Technology*, *27*(5), 943–949. <https://doi.org/10.1175/2009JTECHO704.1>
- Guinet, C., Vacquié-Garcia, J., Picard, B., Bessigneul, G., Lebras, Y., Dragon, A. C., et al. (2014). Southern elephant seal foraging success in relation to temperature and light conditions: Insight into prey distribution. *Marine Ecology Progress Series*, *499*, 285–301. <https://doi.org/10.3354/meps10660>
- Hays, G. C. (2003). A review of the adaptive significance and ecosystem consequences of zooplankton diel vertical migrations. In *Migrations and dispersal of marine organisms* (pp. 163–170). Dordrecht, Netherlands: Springer. <https://doi.org/10.1023/B:HYDR.0000008476.23617.b0>
- Hindell, M. A., Reisinger, R. R., Ropert-Coudert, Y., Hückstädt, L. A., Trathan, P. N., Bornemann, H., et al. (2020). Tracking of marine predators to protect Southern Ocean ecosystems. *Nature*, *580*(7801), 87–92. <https://doi.org/10.1038/s41586-020-2126-y>
- Jaud, T., Dragon, A. C., Garcia, J. V., & Guinet, C. (2012). Relationship between chlorophyll a concentration, light attenuation and diving depth of the southern elephant seal *Mirounga leonina*. *PLoS One*, *7*(10), e47444. <https://doi.org/10.1371/journal.pone.0047444>
- Kaartvedt, S., Røstad, A., Klevjer, T. A., & Staby, A. (2009). Use of bottom-mounted echo sounders in exploring behavior of mesopelagic fishes. *Marine Ecology Progress Series*, *395*, 109–118. <https://doi.org/10.3354/meps08174>
- Kaartvedt, S., Staby, A., & Aksnes, D. L. (2012). Efficient trawl avoidance by mesopelagic fishes causes large underestimation of their biomass. *Marine Ecology Progress Series*, *456*, 1–6. <https://doi.org/10.3354/meps09785>
- Klages, N. T. W., & Bester, M. N. (1998). Fish prey of fur seals *Arctocephalus* spp. at subantarctic Marion Island. *Marine Biology*, *131*(3), 559–566. <https://doi.org/10.1007/s002270050348>
- Klevjer, T. A., Irigoien, X., Røstad, A., Fraile-Nuez, E., Benítez-Barríos, V. M., & Kaartvedt, S. (2016). Large scale patterns in vertical distribution and behaviour of mesopelagic scattering layers. *Scientific Reports*, *6*, 19873. <https://doi.org/10.1038/srep19873>
- Kloser, R. J., Ryan, T. E., Keith, G., & Gershwin, L. (2016). Deep-scattering layer, gas-bladder density, and size estimates using a two-frequency acoustic and optical probe. *ICES Journal of Marine Science*, *73*(8), 2037–2048. <https://doi.org/10.1093/icesjms/fsv257>
- Kloser, R. J., Ryan, T. E., Young, J. W., & Lewis, M. E. (2009). Acoustic observations of micronekton fish on the scale of an ocean basin: Potential and challenges. *ICES Journal of Marine Science*, *66*(6), 998–1006. <https://doi.org/10.1093/icesjms/fsp077>
- Kunath, H., Kloser, R. J., Ryan, T. E., Downie, R. A., Keith, G., & Nau, A. W. (2021). Sounding out life in the deep using acoustic data from ships of opportunity. *Scientific Data*, *8*(1), 23. <https://doi.org/10.1038/s41597-020-00785-8>
- Ladroit, Y., Escobar-Flores, P. C., Schimel, A. C., & O'Driscoll, R. L. (2020). ESP3: An open-source software for the quantitative processing of hydro-acoustic data. *SoftwareX*, *12*, 100581. <https://doi.org/10.1016/j.softx.2020.100581>
- MacLennan, D. N., Fernandes, P. G., & Dalen, J. (2002). A consistent approach to definitions and symbols in fisheries acoustics. *ICES Journal of Marine Science*, *59*(2), 365–369. <https://doi.org/10.1006/jmsc.2001.1158>
- Martínez-Moreno, J., Hogg, A. M., England, M. H., Constantinou, N. C., Kiss, A. E., & Morrison, A. K. (2021). Global changes in oceanic mesoscale currents over the satellite altimetry record. *Nature Climate Change*, *11*(5), 397–403. <https://doi.org/10.1038/s41558-021-01006-9>
- McMahon, C. R., Hindell, M. A., Charrassin, J. B., Corney, S., Guinet, C., Harcourt, R., et al. (2019). Finding mesopelagic prey in a changing Southern Ocean. *Scientific Reports*, *9*(1), 19013. <https://doi.org/10.1038/s41598-019-55152-4>
- Moreau, S., Della Penna, A., Llort, J., Patel, R., Langlais, C., Boyd, P. W., et al. (2017). Eddy-induced carbon transport across the Antarctic Circumpolar Current. *Global Biogeochemical Cycles*, *31*, 1368–1386. <https://doi.org/10.1002/2017GB005669>

- Murphy, E. J., Cavanagh, R. D., Drinkwater, K. F., Grant, S. M., Heymans, J. J., Hofmann, E. E., et al. (2016). Understanding the structure and functioning of polar pelagic ecosystems to predict the impacts of change. *Proceedings of the Royal Society B: Biological Sciences*, 283(1844), 20161646. <https://doi.org/10.1098/rspb.2016.1646>
- Nelson, D. M., & Smith, W. O., Jr. (1991). Sverdrup revisited: Critical depths, maximum chlorophyll levels, and the control of Southern Ocean productivity by the irradiance-mixing regime. *Limnology & Oceanography*, 36(8), 1650–1661. <https://doi.org/10.4319/lo.1991.36.8.1650>
- Oliver, M. P., Hulley, P. A., Castellón, A., Emelianov, M., López, C., Tuset, V. M., et al. (2017). Mesopelagic fishes across the tropical and equatorial Atlantic: Biogeographical and vertical patterns. *Progress in Oceanography*, 151, 116–137. <https://doi.org/10.1016/j.pocean.2016.12.001>
- Omand, M. M., Steinberg, D. K., & Stamieszkin, K. (2021). Cloud shadows drive vertical migrations of deep-dwelling marine life. *Proceedings of the National Academy of Sciences*, 118(32), e2022977118. <https://doi.org/10.1073/pnas.2022977118>
- Orselli, I. B., Kerr, R., de Azevedo, J. L., Galdino, F., Araujo, M., & Garcia, C. A. (2019). The sea-air CO₂ net fluxes in the South Atlantic Ocean and the role played by Agulhas eddies. *Progress in Oceanography*, 170, 40–52. <https://doi.org/10.1016/j.pocean.2018.10.006>
- O'Toole, M., Guinet, C., Lea, M. A., & Hindell, M. A. (2017). Marine predators and phytoplankton: How elephant seals use the recurrent Kerguelen plume. *Marine Ecology Progress Series*, 581, 215–227. <https://doi.org/10.3354/meps12312>
- Patel, R. S., Llorc, J., Strutton, P. G., Phillips, H. E., Moreau, S., Conde Pardo, P., & Lenton, A. (2020). The biogeochemical structure of Southern Ocean mesoscale eddies. *Journal of Geophysical Research: Oceans*, 125, e2020JC016115. <https://doi.org/10.1029/2020JC016115>
- Patel, R. S., Phillips, H. E., Strutton, P. G., Lenton, A., & Llorc, J. (2019). Meridional heat and salt transport across the Subantarctic Front by cold-core eddies. *Journal of Geophysical Research: Oceans*, 124, 981–1004. <https://doi.org/10.1029/2018JC014655>
- Picco, P., Schiano, M. E., Pensieri, S., & Bozzano, R. (2017). Time-frequency analysis of migrating zooplankton in the Terra Nova bay polynya (Ross Sea, Antarctica). *Journal of Marine Systems*, 166, 172–183. <https://doi.org/10.1016/j.jmarsys.2016.07.010>
- Proud, R., Cox, M. J., & Brierley, A. S. (2017). Biogeography of the global ocean's mesopelagic zone. *Current Biology*, 27(1), 113–119. <https://doi.org/10.1016/j.cub.2016.11.003>
- Proud, R., Cox, M. J., Wotherspoon, S., & Brierley, A. S. (2015). A method for identifying sound scattering layers and extracting key characteristics. *Methods in Ecology and Evolution*, 6(10), 1190–1198. <https://doi.org/10.3354/meps12612>
- Receveur, A., Kestenare, E., Allain, V., Ménard, F., Cravatte, S., Lebourges-Dhaussy, A., et al. (2020). Micronekton distribution in the southwest Pacific (New Caledonia) inferred from shipboard-ADCP backscatter data. *Deep Sea Research Part I: Oceanographic Research Papers*, 159, 103237. <https://doi.org/10.1016/j.dsr.2020.103237>
- Rohr, T., Harrison, C., Long, M. C., Gaube, P., & Doney, S. C. (2020a). The simulated biological response to Southern Ocean eddies via biological rate modification and physical transport. *Global Biogeochemical Cycles*, 34, e2019GB006385. <https://doi.org/10.1029/2019GB006385>
- Rohr, T., Harrison, C., Long, M. C., Gaube, P., & Doney, S. C. (2020b). Eddy-modified iron, light, and phytoplankton cell division rates in the simulated Southern Ocean. *Global Biogeochemical Cycles*, 34, e2019GB006380. <https://doi.org/10.1029/2019GB006380>
- Røstad, A., Kaartvedt, S., & Aksnes, D. L. (2016). Light comfort zones of mesopelagic acoustic scattering layers in two contrasting optical environments. *Deep Sea Research Part I: Oceanographic Research Papers*, 113, 1–6. <https://doi.org/10.1016/j.dsr.2016.02.020>
- Ryan, T. E., Kloser, R. J., & Macaulay, G. J. (2009). Measurement and visual verification of fish target strength using an acoustic-optical system attached to a trawlnet. *ICES Journal of Marine Science*, 66(6), 1238–1244. <https://doi.org/10.1093/icesjms/fsp122>
- Sokolov, S., & Rintoul, S. R. (2009). Circumpolar structure and distribution of the Antarctic Circumpolar Current fronts: 1. Mean circumpolar paths. *Journal of Geophysical Research*, 114, C11018. <https://doi.org/10.1029/2008JC005108>
- Son, S., & Wang, M. (2015). Diffuse attenuation coefficient of the photosynthetically available radiation K_d (PAR) for global open ocean and coastal waters. *Remote Sensing of Environment*, 159, 250–258. <https://doi.org/10.1016/j.rse.2014.12.011>
- Subramaniam, R. C., Corney, S. P., Swadling, K. M., & Melbourne-Thomas, J. (2020). Exploring ecosystem structure and function of the northern Kerguelen Plateau using a mass-balanced food web model. *Deep Sea Research Part II: Topical Studies in Oceanography*, 174, 104787. <https://doi.org/10.1016/j.dsr2.2020.104787>
- Sutton, T. T., Clark, M. R., Dunn, D. C., Halpin, P. N., Rogers, A. D., Guinotte, J., et al. (2017). A global biogeographic classification of the mesopelagic zone. *Deep Sea Research Part I: Oceanographic Research Papers*, 126, 85–102. <https://doi.org/10.1016/j.dsr.2017.05.006>
- Tew-Kai, E., Rossi, V., Sudre, J., Weimerskirch, H., Lopez, C., Hernandez-Garcia, E., et al. (2009). Top marine predators track Lagrangian coherent structures. *Proceedings of the National Academy of Sciences of the United States of America*, 106(20), 8245–8250. <https://doi.org/10.1073/pnas.0811034106>
- Trenkel, V. M., & Berger, L. (2013). A fisheries acoustic multi-frequency indicator to inform on large scale spatial patterns of aquatic pelagic ecosystems. *Ecological Indicators*, 30, 72–79. <https://doi.org/10.1016/j.ecolind.2013.02.006>
- Trull, T. W., Bray, S. G., Manganini, S. J., Honjo, S., & Francois, R. (2001). Moored sediment trap measurements of carbon export in the Subantarctic and Polar Frontal Zones of the Southern Ocean, south of Australia. *Journal of Geophysical Research*, 106(C12), 31489–31509. <https://doi.org/10.1029/2000JC000308>
- Urmy, S. S., & Horne, J. K. (2016). Multi-scale responses of scattering layers to environmental variability in Monterey Bay, California. *Deep Sea Research Part I: Oceanographic Research Papers*, 113, 22–32. <https://doi.org/10.1016/j.dsr.2016.04.004>
- Watanuki, Y., & Thiebot, J. B. (2018). Factors affecting the importance of myctophids in the diet of the world's seabirds. *Marine Biology*, 165(4), 79. <https://doi.org/10.1007/s00227-018-3334-y>
- Wiebe, P. H., Morton, A. W., Bradley, A. M., Backus, R. H., Craddock, J. E., Barber, V., et al. (1985). New development in the MOCNESS, an apparatus for sampling zooplankton and micronekton. *Marine Biology*, 87(3), 313–323. <https://doi.org/10.1007/BF00397811>